

Computational Study of Room-Temperature Ionic Liquids Interacting with a POPC Phospholipid Bilayer

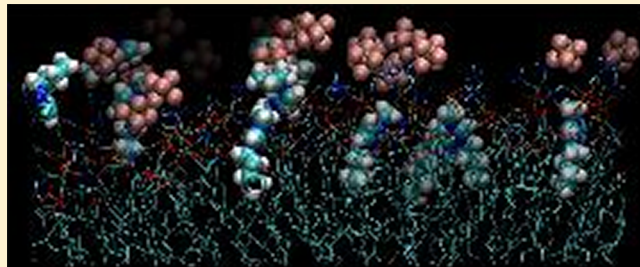
Richard J. Bingham^{*,†} and Pietro Ballone[‡]

[†]Centre for Molecular Nanoscience, School of Chemistry, University of Leeds, Leeds LS2 9JT, United Kingdom

[‡]Centre Européen de Calcul Atomique et Moléculaire, EPFL, Lausanne, Switzerland

Supporting Information

ABSTRACT: Molecular dynamics simulations based on an empirical force field have been carried out to investigate the properties of a zwitter-ionic phospholipid (POPC) bilayer in contact with a water solution of $[bmim][Cl]$, $[bmim][PF_6]$ and $[bmim][Tf_2N]$ at concentration $c = 0.5$ M. The results reveal important and specific interactions of cations and anions with the bilayer. The $[bmim]^+$ cation, in particular, shows a clear tendency to be incorporated tail-first into the bilayer. $[Cl]^-$ remains in solution, $[PF_6]^-$ forms a thin layer on the lipid surface, and $[bmim][Tf_2N]$ precipitates out of the solution, giving rise to an ionic droplet deposited on the lipid surface. The simulation results provide a microscopic basis to interpret the available experimental observations.



I. INTRODUCTION

Room temperature ionic liquids (RTILs)¹ have been extensively investigated in recent years because of their peculiar chemical-physics properties, making them promising candidates for a wide range of applications. These include electrochemistry, with RTILs playing the role of advanced electrolytes in batteries,² fuel cells,³ and dye-sensitized solar cells,⁴ but also catalysis⁵ and lubrication,⁶ not to mention exotic applications in CO_2 sequestration⁷ and as a flexible and controllable medium in lunar-based telescopes.⁸

From a practical and economic point of view, however, the most important applications of RTILs could be as a replacement of water-based or neutral organic solvents in a variety of industrial chemical processes.⁹ On average, RTILs are more expensive than the solvents they are supposed to replace, but their low volatility greatly limits their dispersion in the environment, reducing waste and decreasing pollution.¹⁰ Together with their flexibility and tunability, arising from the chemical variety and countless number of these compounds, this property could easily offset the initial cost of RTILs.

Despite their environmental-friendly label, or, perhaps, even more because of it, it is still necessary and urgent to assess the biological effects of RTILs,¹¹ since a widespread usage in chemical processes will certainly result in their routine or accidental release in the environment. The interaction of RTILs with complex biological structures, moreover, is of interest for the realization of biocatalytic systems in nonaqueous environments, especially of those made of enzymes embedded in lipid bilayers deposited on surfaces, and involving RTILs as solvents for substrates and products.^{12,13}

Recent studies have shown that RTILs are compatible with enzyme activity.¹⁴ Health safety, however, is a much more

complex issue. Concerns about the biological effects of these compounds, in particular, have been raised by the results of a toxicology study on zebrafish.^{15,16} Most RTILs displayed fairly low toxicity, but a few of them had a drastic negative effect on fish survival. Fortunately, the relevance of these observations is somewhat mitigated by the fact that the RTIL concentrations in the environment resulting from industrial processes operating at normal conditions are expected to be much lower than the value needed to kill a statistically significant portion of the fish in the laboratory tests.

A broader impact of RTILs on health, however, could be foreseen on the basis of a series of experimental studies^{17,12,18} using atomic force microscopy (AFM), fluorescence, and quartz crystal microbalance measurements to investigate the interaction of RTILs with lipid vesicles and surface-supported phospholipid bilayers. Since biomembranes consist primarily of lipid bilayers, these artificial systems can be considered as idealized models for the interaction of RTILs with the protective envelope of cells.

The results of these studies revealed important and specific interactions of RTILs with zwitterionic phospholipids, affecting basic properties of the bilayers, in some cases undermining their integrity. Fluorescence spectroscopy, in particular, has been used to detect leakage from lipid vesicles following the addition of 1-alkyl-3-methylimidazolium salts in solution.¹⁷ The effect of cations and anions has been disentangled by coupling each RTIL species with a simple inorganic counterion such as $[Li]^+$ or $[Cl]^-$, whose interaction with lipids is known to be fairly

Received: June 21, 2012

Revised: August 8, 2012

Published: August 20, 2012

weak. Results show that the imidazolium cations are incorporated into the bilayer, causing disruptions whose relevance increases with the length of the alkyl side chain. Anions such as $[\text{Cl}]^-$ and $[\text{PF}_6]^-$ had little effect on the vesicles' integrity, whereas $[\text{Tf}_2\text{N}]^-$ at 500 mM concentration produced holes giving rise to leakage.

The experimental picture has been completed and reinforced by quartz microbalance measurements and AFM imaging on a phospholipid (DEPC) bilayer supported on a silica surface, showing that 1-octyl-3-methylimidazolium ($[\text{omim}]^+$) removes lipids from the bilayer, and $[\text{Tf}_2\text{N}]^-$ creates large but localized pores.¹⁸ In all cases, increasing the RTILs concentration above their critical micelle concentration (CMC) decreases their effect on lipid bilayers. As expected, interaction and effects of RTILs on phospholipid bilayers were found to be larger in the case of ionic lipids.¹²

The relevance of these observations can be assessed by comparison with the abundant experimental and computational information on phospholipid bilayers in contact with water solutions of simpler inorganic electrolytes such as NaCl, KCl, MgCl_2 , CaCl_2 , etc., for which the interaction can be assumed to be almost purely Coulombic. The global picture arising from these studies is too broad and complex to be summarized here. We only revisit the most basic facts, and we refer to specialized reviews for a detailed discussion.¹⁹ Not surprisingly, the interaction of simple inorganic salts is found to be strong with charged lipids, and moderate with neutral and zwitterionic lipids, which represent ~90% of the lipids in natural biomembranes. Again as expected, interactions with charged and zwitterionic phospholipids are stronger in the case of divalent ions^{20,21} than in the case of monovalent species. Up to fairly high concentrations, none of these simple salts drastically affect the morphology or undermine the stability of the bilayer, although quantitative changes in the structure, dynamics, and phase diagram of phospholipid bilayers upon the solvation of electrolytes are observed in all systems, even in the case of the weakest interactions, i.e., in the zwitterionic phospholipids case in contact with a water solution of NaCl.²²

Despite the obvious interest in this subject and despite the availability of experimental results, the computational investigation of lipid bilayers in water solutions of organic electrolytes such as RTILs is still in its preliminary stage. Recently, we carried out an exploratory investigation of RTILs interactions with bilayers made of the simplest lipid, i.e., cholesterol.²³ The results provided useful insight into the structure and dynamics of the combined RTILs–bilayer system, and on the mechanisms of defects' formation. Moreover, the computational picture displayed several intriguing points of contact with the experimental information obtained in the case of RTIL–phospholipid bilayers. Cholesterol bilayers in water, however, are not relevant for biology, and, at most, represent test cases for chemical physics experiments.²⁴

In this paper we present the results of molecular dynamics simulations of $[\text{bmim}][\text{Cl}]$, $[\text{bmim}][\text{PF}_6]$ and $[\text{bmim}][\text{Tf}_2\text{N}]$ in water solution, interacting with a planar phospholipid (1-palmitoyl-2-oleoyl-sn-glycero-3-phosphocholine, POPC) bilayer. The small set of organic salts considered in our study includes prototypical RTILs, listed in order of increasing hydrophobicity,²⁵ from $[\text{bmim}][\text{Cl}]$, which is fairly soluble, to $[\text{bmim}][\text{Tf}_2\text{N}]$, whose solubility in water at ambient temperature is limited to 15.7 ± 0.2 mM.²⁵ POPC is zwitterionic, and is biologically relevant, being found in the membrane of eukaryote cells.²⁶ Its basic properties are fairly well understood,

since it has been the subject of many experimental and computational studies.^{27–29} Phosphocholine lipids such as POPC, in particular, are responsible for the integrity of biomembranes,³⁰ and thus represent a natural benchmark to assess the potential effect of RTILs.

The length and time scales required to reproduce the extended damage of lipid membranes by RTILs seen in experiments are still beyond the reach of atomistic molecular dynamics simulations. However, even our simulations, covering ~10 nm and ~100 ns, are able to highlight the microscopic origin of the morphology changes undergone by lipid bilayers upon the addition of RTILs. The results of our simulations, in particular, point to specific and fairly strong interactions between RTILs and the POPC bilayer, mediated by a combination of Coulomb and dispersion forces, as well as by subtle entropic effects. On the longer term, the combined knowledge from experiments and from simulation on RTILs/membrane interactions could be relevant not only for the toxicology of these compounds but could also have a beneficial impact on the application of RTILs as active principles in pharmacology.³¹

II. MODEL AND COMPUTATIONAL METHOD

In our study we consider a planar POPC bilayer immersed in a water solution of $[\text{bmim}][\text{Cl}]$, $[\text{bmim}][\text{PF}_6]$, and $[\text{bmim}][\text{Tf}_2\text{N}]$ at ~0.5 M concentration. The schematic structures of POPC, the $[\text{bmim}]^+$ cation, and the anions considered in our study are shown in Figure 1.

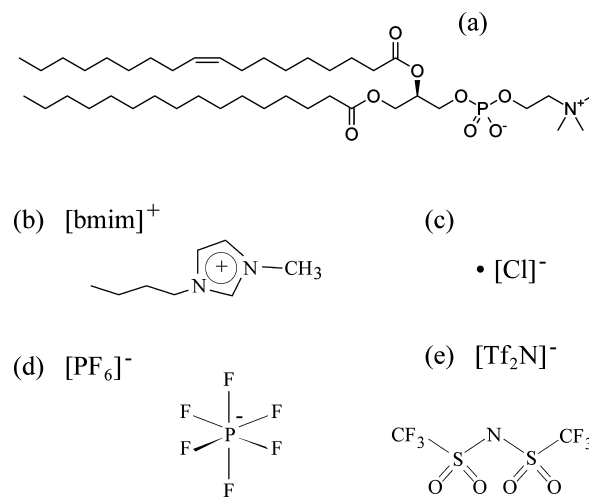


Figure 1. Schematic structures of (a) POPC, (b) $[\text{bmim}]^+$, (c) $[\text{Cl}]^-$, (d) $[\text{PF}_6]^-$, and (e) $[\text{Tf}_2\text{N}]^-$.

POPC is a zwitterionic phospholipid, with a lone $\text{C}=\text{C}$ double bond in the longest (oleoyl acyl chain) of its two hydrocarbon tails. In our simulations, relying on the GROMACS package,³² POPC is described by a united atom model, representing each molecule, consisting of 134 atoms, by 52 particles, having incorporated explicit nonpolar hydrogens into the corresponding aliphatic carbon atoms. For the sake of simplicity, in what follows the representing particles will often be referred to as atoms. Interparticle interactions are described by the Berger lipid model³³ included into the Gromos53a6 force field.³⁴ Atomic charges for POPC have been taken from ref 35.

Water and RTILs are modeled in atomistic detail. For water, in particular, we used the SPC model.³⁶ RTILs species have been described by an Amber/OPLS-type potential, whose parameters for bonded and nonbonded, i.e., Coulomb and van der Waals interactions have been taken from ref 37. The usage of integer ($\pm e$) charges on cations and anions in the model of ref 37 has been criticized in ref 38, showing that reducing the charges to $\pm 0.8e$ per ion provides better values for the diffusion constant and for the surface tension of pure RTILs. We decided in favor of the original model because noninteger charges, introduced to mimic electronic polarization effects in homogeneous and pure-RTIL systems, are more difficult to justify in highly anisotropic systems, or in systems, such as ours, in which dissociated, fully hydrated ions move independently in a predominantly water environment. Moreover, the usage of integer charges in the model of ref 37, to a large extent, has been revalidated in ref 38. Last but not least, this same model with integer charges has been used recently for an extensive investigation of water-RTIL solutions over the entire concentration range.⁴⁰

All van der Waals cross interactions have been defined using the geometric-average Berthelot's rule:

$$\epsilon_{ij} = \sqrt{\epsilon_{ii}\epsilon_{jj}} \quad (1)$$

$$\sigma_{ij} = \sqrt{\sigma_{ii}\sigma_{jj}} \quad (2)$$

The mutual compatibility of the RTIL and phospholipid models relies on their separate compatibility with the same water model.^{40,41} Unfortunately, no direct verification on the quality of the RTIL/POPC interaction model is possible at this stage.

At a more technical level, as already pointed out by other authors,⁴² we observe that the Amber/OPLS form of the RTIL force field is somewhat inconsistent with the Gromos form of the Berger potential for lipids. The problem arises from the so-called 1–4 interactions within each set, which concern pairs of atoms belonging to the same molecule and separated by three covalent bonds. These interactions include both van der Waals (Lennard-Jones, LJ) and Coulomb contributions,³² and may become exceedingly large since 1–4 distances can be fairly short. To control their size, GROMACS uses two parameters to rescale 1–4 interactions, these being referred to as fudge factors. The fudge factor *fudgeQQ* used to scale Coulombic contributions is applied to all 1–4 pairs, whereas the Lennard-Jones scaling *fudgeLJ* is only applied to the 1–4 interactions whose LJ parameters are not explicitly given in the input.

The Berger potential for lipids³³ specifies all LJ parameters for the 1–4 interactions, and assumes full Coulomb interactions (*fudgeQQ* = 1) among 1–4 pairs. The Amber/OPLS potential, instead, sets *fudgeLJ* = *fudgeQQ* = 0.5 for all 1–4 interactions.

To solve this conflict, in our GROMACS input we use the fudge parameters from the Amber/OPLS potential, (*fudgeLJ* = *fudgeQQ* = 0.5), which means we can use the Amber/OPLS parameter set without any changes. To ensure that the 1–4 interactions in the Berger-lipid set are still accounted for correctly, we change the way in which they are calculated. As the *fudgeQQ* factor we used is half of the value that the parameter set is designed for, we extend the list of 1–4 pairs so that each 1–4 interaction is calculated twice. This restores the 1–4 Coulombic contribution to the original magnitude. The Berger-lipid set does not use *fudgeLJ* scaling, as the LJ parameters for the 1–4 interactions are specified in the input;

therefore, the Lennard-Jones contribution to the 1–4 interaction is now exactly double what it should be. To restore its original magnitude, we divide by two the corresponding ϵ_{ij} parameters.

A different strategy to achieve the same matching of the Berger model with the Gromos potentials of peptides and proteins was proposed by Tieleman,⁴² incorporating all of the 1–4 interactions into the dihedral term, thus making the lipid potential insensitive to the choice of the fudge factors.

The simulated sample is enclosed in an orthorhombic cell, with periodic boundary conditions applied. Coulomb interactions are computed using the particle-mesh Ewald algorithm.⁴³ Following the accepted practice, the Lennard-Jones potentials are cut off at 1.2 nm. The same cutoff distance is used for the real space part of the Ewald summation. This second cutoff is less relevant than the first, since it only decides the relative weight of real- and reciprocal-space contribution to the Coulomb energy, leaving unchanged the sum of the two. All bond distances are kept fixed using the LINCS algorithm.⁴⁴

Simulations have been carried out in the NPT ensemble at $T = 300$ K and $P = 1$ atm, using a Nosé-Hoover thermostat and a Parrinello-Rahman semi-isotropic pressure coupling,⁴⁵ with a time constant of 0.5 ps throughout. Equations of motion have been integrated using the leapfrog (Verlet) algorithm, with a time step $\delta t = 1$ fs.

The GROMACS simulation package³² in the 4.5.5/4.5.3 version, running in parallel on the HECToR supercomputer, has been used for all simulations. Most of the runs used 4 nodes, with a total of 128 CPU's. A typical run, involving samples consisting of about 70 000 atoms, required 80 h on 4 nodes to cover 20 ns. Initial configurations and input files have been prepared and modified using a combination of GROMACS utilities and home-built Fortran programs.

The instantaneous value of the area A covered by the bilayer is measured by the xy cross section of the simulation box. The mean square fluctuation σ_A^2 of A around its average value $\langle A \rangle$ is used to estimate the surface compressibility modulus,⁴⁶ i.e., an inverse area compressibility, of the bilayer, given by:

$$\kappa_A = \frac{\langle A \rangle k_B T}{\sigma_A^2} \quad (3)$$

where k_B is the Boltzmann constant. Corrections due to the undulation of the bilayer⁴⁶ have not been applied, even though it has been shown⁴⁶ that neglecting these undulation contributions leads to a slight underestimation of $\langle A \rangle$ and to a somewhat more significant overestimation of κ_A . In the present study, however, we are interested more in the variations of these quantities upon the addition of RTILs in solution than in their absolute value, and the simplest method we adopt is adequate for our purposes.

The instantaneous position of the geometric surface separating water from the POPC bilayer has been defined taking the lipid position as a reference. For each configuration, a test particle of $\sigma_t = 3$ Å diameter has been moved along the z direction, starting from a position (x_0, y_0, z_0) well above the bilayer. At constant (x_0, y_0) the test particle is lowered along z toward the bilayer in steps of 0.5 Å, until the first particle belonging to the lipid is found within a distance σ_t from the center of the test particle. The corresponding height $(z - \sigma_t/2)$ provides a (slightly discretized) estimate of the instantaneous position $Z_U(x_0, y_0, t)$ of the upper interface at time t . The downward shift of $\sigma_t/2$ from z to Z_U , of course, accounts for the

finite size of the probe particle. This procedure is repeated for all of the (x_0, y_0) points on a 64×64 regular grid in the xy plane and replicated again for the lower surface, starting from a z_0 well below the bilayer and moving upward until first contact at height z with particles belonging to phospholipid molecules, thus locating the lower surface at $Z_L(x_0, y_0, t) = z + \sigma_t/2$. In the case of RTIL solutions, the precise definition of the lipid/water separation surface may be blurred by the segregation of cations and/or anions at the POPC surface, but Z_U and Z_L remain an accurate representation of the surfaces limiting the lipid bilayer.

The difference $\Delta_t = \{[Z_U(x, y, t) - Z_L(x, y, t)] - \sigma_t\}$ is an xy -dependent estimate of the bilayer thickness. Once integrated over the simulation box cross section, which also fluctuates, it provides a measure of the instantaneous volume V_t occupied by the bilayer. The mean square fluctuation of this volume ($\sigma_{V_t}^2$) around its average value $\langle V_t \rangle$, in turn, allow us to determine the isothermal compressibility of the phospholipid bilayer, according to

$$\chi_T = \frac{\sigma_{V_t}^2}{k_B T \langle V_t \rangle} \quad (4)$$

where it is assumed that σ^2 and $\langle V_t \rangle$ are computed by simulations in the NPT ensemble.

Different definition of the bilayer thickness, and thus of the phospholipid volume, are often used in the literature. Examples include the separation of the average phosphorus plane in the two leaflets, and the so-called Luzzati thickness and Luzzati volume, defined in terms of the water density profile.⁴¹ While these last two volumes are only briefly commented on later, in what follows we use yet another definition of the volume ($V_{\Omega-w}$) of the phospholipid bilayer, given by the difference between the average system volume, and the average volume occupied by water at the same (P, T) conditions. This last volume, in turn, is defined as the number of water molecules in the sample times the average volume per molecule estimated by an independent simulation of pure water, again at the same thermodynamic conditions. In our simulations, the average volume of water at $T = 300$ K and $P = 1$ atm turns out to be $v_w = 2.997 \pm 0.002 \times 10^{-2}$ nm³ per molecule. In a similar way, we define the volume of each cation–anion pair considered in our simulations, computed by subtracting the water volume from the average volume of a homogeneous RTIL–water solution. We obtain in this way: $v([bmim][Cl]) = 0.2683 \pm 0.0002$ nm³ and $v([bmim][PF_6]) = 0.34745 \pm 0.0001$ nm³, again at $T = 300$ K, $P = 1$, and concentration comparable to that of the main simulations. The third RTIL, i.e., [bmim][Tf₂N], does not give rise to a homogeneous solution in water at the conditions of our simulation.

The instantaneous position of the upper and lower interfaces can be Fourier transformed in the xy plane, and then expressed as a linear combination of planes waves

$$Z_{U(L)}(x, y) = \sum_{\mathbf{q}} c_{\mathbf{q}}^{U(L)} e^{i\mathbf{qr}_{||}} \quad (5)$$

where the U or L labels refer to the upper and lower surface, respectively, $r_{||} \equiv (x, y)$, the $\{\mathbf{q}\}$ vectors are 2D reciprocal lattice vectors of the simulation cell in the xy plane, and of course

$$c_{\mathbf{q}}^{U(L)}(t) = \frac{1}{A} \int_A Z_{U(L)}(x, y, t) e^{-i\mathbf{qr}_{||}} dr_{||} \quad (6)$$

where A is the cross section area, i.e., the area of the xy face of the simulation cell, which is itself a function of time t .

Simple statistical mechanics arguments relate the thermal average $\langle c_{\mathbf{q}} c_{-\mathbf{q}} \rangle$ to thermodynamics quantities, according to^{46,47}

$$\langle c_{\mathbf{q}} c_{-\mathbf{q}} \rangle = \frac{k_B T}{A} \frac{1}{\gamma q^2 + k_c q^4} \quad (7)$$

where γ is the interfacial tension and k_c is the bending rigidity of the bilayer. The U or L superscripts have been dropped here because, once averaged over time, the upper and lower surface are equivalent. Then, a plot of $\langle c_{\mathbf{q}} c_{-\mathbf{q}} \rangle$ as a function of q on a semilogarithmic scale allows us to determine the interfacial tension γ by a linear fit of the long wavelength portion of $\log \langle c_{\mathbf{q}} c_{-\mathbf{q}} \rangle$ as a function of q , following a procedure already used several times in the literature.⁴⁸

The electrostatic potential along the direction z perpendicular to the bilayer is computed from the charge density distribution $\rho_Q(z)$ averaged over time, according to

$$\psi(z) - \psi(z_0) = -\frac{1}{\epsilon_0} \int_{z_0}^z (z - z') \rho_Q(z') dz' \quad (8)$$

where ϵ_0 is the permittivity of vacuum and z_0 is a position well inside the water slab, with $\rho_Q(z_0) = 0$.

The deuterium order parameter S_{CD} measures the orientation of individual carbon–deuterium bonds with respect to the bilayer normal, i.e., the z axis in our computation, and is used below to characterize the phase of the POPC sample. For each methylene group i in the phospholipid tail, the S_{CD} order parameter is given by

$$S_{CD}^i = \frac{1}{2} \langle 3\cos^2 \theta_i - 1 \rangle \quad (9)$$

where θ_i is the angle between the C–D bond and the \hat{z} direction. The united atom representation used by GROMACS complicates somewhat the computation of S_{CD}^i , that, however, is made possible by standard assumptions on the local bonding geometry of the POPC hydrocarbon tails (see ref 41 for more details).

III. SIMULATION RESULTS

A. POPC Bilayer in Pure Water. Our simulations have been started from a configuration obtained from the Web site of ref 42, giving the coordinates of a planar $M = 340$ -molecules POPC bilayer equilibrated in ~ 7000 water molecules. At the moderate RTILs concentrations of interest for our study (0.5M), a water bath of this size corresponds to ~ 60 ion pair. At these low numbers, the adsorption on or the incorporation into the bilayer of even a few ions would change significantly their density in solution, thus altering the reference electrolyte concentration. Moreover, average quantities such as the charge density profile or the electrostatic potential drop at the interface would be affected by large statistical uncertainties. To overcome these problems, we enlarged our system, increasing the number of water molecules to 17 789, corresponding to ~ 52 water molecules per POPC molecule and then to nearly one ion pair every two lipid molecules. The extended sample has been briefly re-equilibrated over a few ns. At this stage, the simulation box is about $L_x \times L_y \times L_z = 10 \times 10 \times 9.5$ nm³, with the bilayer lying in the xy plane.

To provide a benchmark for the simulations with RTILs in solution, the POPC bilayer in pure water has been simulated for a total of 140 ns at $T = 300$ K and $P = 1$ atm. Average quantities, to be compared with those obtained upon the addition of RTILs, have been computed over the last 110 ns of

this long trajectory (see Table 1). The bilayer expanded slightly without any apparent morphology change during the

Table 1. Total Simulation Time and Statistics Time for the Systems Considered in Our Study, Consisting of a POPC Bilayer in Contact with the Solutions Listed in the Table Heading, where *w* is an Abbreviation for Water

sample	<i>w</i>	[bmim][Cl]/ <i>w</i>	[bmim][PF ₆]/ <i>w</i>	[bmim][Tf ₂ N]/ <i>w</i> (0.5 M)	[bmim][Tf ₂ N]/ <i>w</i> (0.25 M)
tot. (ns)	140	110	110	90	40
stat. (ns)	110	80	80	60	10

equilibration stage and remained stationary during the long production run. A simulation snapshot of the POPC bilayer in pure water is shown in Figure 2. The penetration of water into

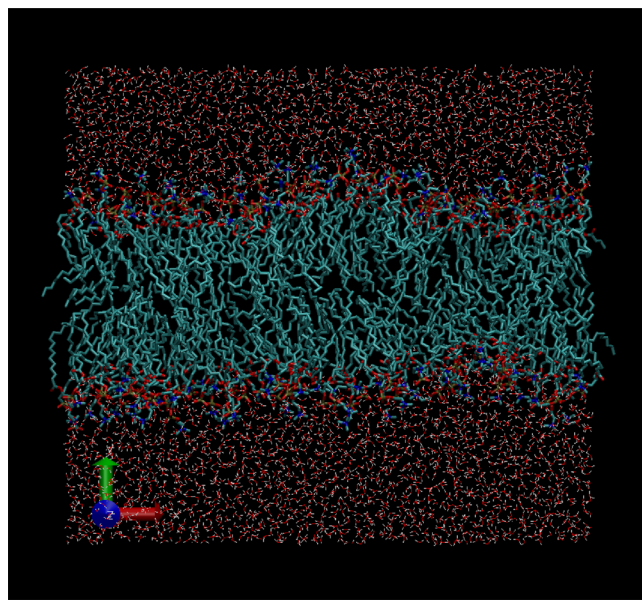


Figure 2. Simulation snapshot of the POPC bilayer in pure water.

the inner portion of the POPC bilayer is negligible, even though not strictly absent. Analysis of configurations shows that the hydration of the POPC headgroup is consistent with the results of previous studies.⁴¹

The first relevant question concerns the equilibrium phase for the simulated sample, since we are interested in the disordered liquid phase *L*_d, which, in real life, is stable above *T*_d = 270 K and for this reason is the most relevant one from the biology point of view. To determine the phase of our sample, following the suggestion of ref 41, we analyze several diagnostic properties. Nearly all of them unambiguously point to the correct *L*_d phase. The only slight deviations from this pattern are observed for the quantities easiest to compute, such as the surface area and the surface compressibility modulus. The surface area per lipid (in each leaflet), for instance, turns out to

be equal to *A*₁ = 2⟨*A*⟩/*M* = 0.597 ± 0.0005 nm², i.e., somewhat below the most recent simulation value⁴¹ (*A*₁ = 0.638 nm² at *T* = 303 K) for the *L*_d phase⁴⁹ but still within the broad interval spanned by experimental data, ranging from *A*₁ = 0.54 nm² at *T* = 275 K of ref 50, to *A*₁ = 0.63 nm² at *T* = 297 K (ref 51), or *A*₁ = 0.683 nm² at *T* = 303 K from ref 27. The computed surface compressibility modulus, $\kappa_A = 590 \pm 5$ mN/m, is higher than the experimental value ($\kappa_A = 231 \pm 20$ mN/m from ref 28) but within the range of previous simulation results for the *L*_d phase. On the other hand, visual analysis of the structure (Figure 2) shows the type of disorder expected for the *L*_d phase, the lipid diffusion, computed from the mean-square displacement of the P atoms (see Table 2), turns out to be *D*_P = 1.6 ± 0.5 × 10⁻⁸ m²/s, and thus, it is within the liquid range for molecules of the POPC size. Moreover, the density profiles for all species (Figure 3) are relatively structureless, as seen in the *L*_d phase,

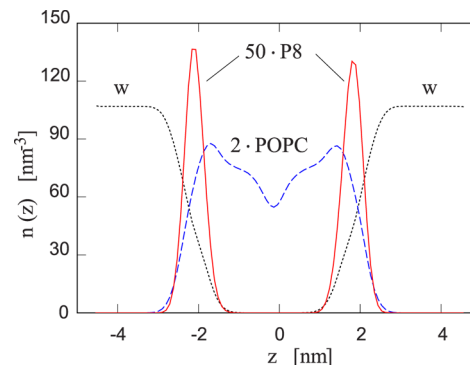


Figure 3. Density distribution of atoms from water molecules (w), POPC particles (POPC), and phosphorus atoms (P8) along the direction *z* perpendicular to the bilayer. The POPC and P8 densities have been rescaled for the sake of clarity.

and at variance from the results for the gel phase. Finally, and perhaps more importantly, the NMR deuterium order parameter shown in Figure 4 is very close to the results obtained in previous simulations⁴¹ and experiments⁵² and significantly lower than data measured on the gel phase. On the basis of these observations, we are confident that the sample considered in our simulations is indeed in the *L*_d phase.

All other quantities computed during our simulations are consistent with this conclusion, and agree with previous simulation results. The 10–90% width of the water density profile in Figure 3 is fairly wide (Δ_{10}^{90} = 1.15 nm), resulting from the hydration of the phospholipid head groups and, possibly, reflecting large amplitude, low frequency oscillations of the bilayer. The interfacial tension $\gamma \approx 0.2$ mN/m is 2 orders of magnitude lower than that of the free water surface ($\gamma = 71$ mN/m at *T* = 305 K⁵³), in agreement with a well-known condition ($\gamma \approx 0$) for the equilibrium area of the interface.

Despite the low value of γ , the water–lipid interface is fairly smooth, as shown in Figure 5, apparently stabilized by higher-order terms in the denominator of eq 7.

The volume *V*₁ per lipid molecule computed from $\Delta_t = \{ |Z_U - Z_L| - \sigma_i \}$ turns out to be *V*₁ = *V*_t/*M* = 1.1876 ± 3 × 10⁻⁴

Table 2. Diffusion Coefficient of Phospholipids Estimated from the Mean Square Displacement of the P Atoms of the POPC Bilayer in Pure Water (w) and in the RTIL/w Solutions

solvent	w	[bmim][Cl]/ <i>w</i>	[bmim][PF ₆]/ <i>w</i> (0.5 M)	[bmim][Tf ₂ N]/ <i>w</i> (0.25 M)	[bmim][Tf ₂ N]/ <i>w</i>
<i>D</i> /10 ⁻⁸ (m ² /s)	1.6 ± 0.5	2.2 ± 0.2	1.6 ± 0.2	2.0 ± 0.5	1.9 ± 0.8

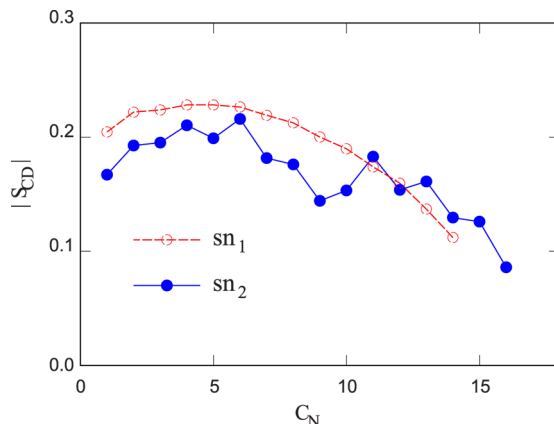


Figure 4. Deuterium order parameter S_{DC} of POPC computed by simulation for the bilayer in pure water. The sn_1 and sn_2 labels refer to the palmitoyl and oleoyl acyl chains of POPC, respectively.

nm^3 , whereas the estimate $V_{\Omega-w}$ based on the complementary volume of lipids and water gives $V_{\Omega-w} = 1.206 \pm 5 \times 10^{-4} \text{ nm}^3$. The estimate based on the average position of the P atoms, and the Luzzati volume both give a value very close to V_t . On computational grounds, we prefer the V_t estimate, which in our opinion better reflects the microscopic structure of the bilayer. Experiments, however, measure a quantity closer to $V_{\Omega-w}$, giving values from $V_{\text{exp}} = 1.229 \text{ nm}^3$ (ref 54) to $V_{\text{exp}} = 1.232 \text{ nm}^3$ (ref 55).

The electrostatic signature of the bilayer, represented by the charge density profile and electrostatic potential across the interface, are shown in Figure 6. The potential energy difference between the center of the lipid bilayer and the center of the water slab turns out to be $\Delta\psi = 0.58 \text{ V}$, in line with previous computations, and resulting from the near compensation of two larger contributions of opposite sign due to POPC and to water.

B. POPC Bilayer in Contact with RTIL Solutions. Samples consisting of a POPC bilayer in contact with a water solution of [bmim][Cl], [bmim][PF₆], or [bmim][Tf₂N] have been prepared starting from a well equilibrated configuration of the neat POPC–water case, by (1) removing water, retaining

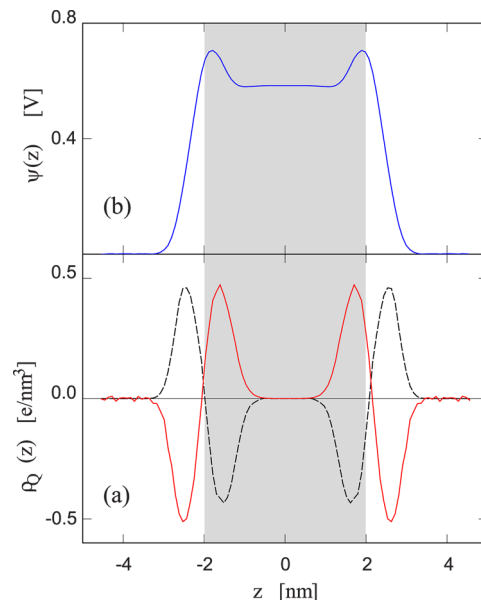


Figure 6. (a) Charge density distribution along the direction z perpendicular to the bilayer, due to POPC (full line, blue), water (dash line, red), (b) electrostatic potential $\psi(z)$ due to the total charge density. The shaded area corresponds to the average width of the bilayer, determined by the test-particle method (see text).

only those H₂O molecules whose distance from lipid atoms was less than 3 Å, (2) adding single RTIL ions at random positions and orientations, rejecting all insertions such that the minimum distance of RTIL and POPC atoms was less than 5 Å, and (3) reinserting water using standard GROMACS utilities. Retaining a thin (3 Å) water layer at contact and avoiding insertions at close range both had the aim of limiting the disruption of the equilibrated lipid bilayer while adding the ions. In all cases, the same number (160) of ion pairs has been added to the system. However, the procedure used by GROMACS to add water resulted in slightly different numbers of water molecules in the three cases, corresponding to 18 745 water molecules in the case of [bmim][Cl], 19 428 water molecules for [bmim][PF₆], and 18 686 water molecules for [bmim][Tf₂N]. These differences in the number of water molecules are relatively

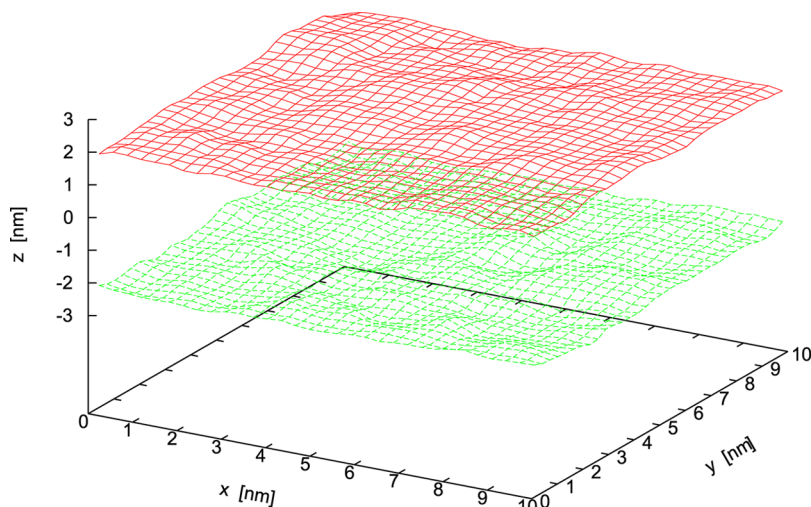


Figure 5. Simulation snapshot of the geometric lipid/water interface of POPC in pure water, identified by the probe-particle construction described in section II. The lipid bilayer occupies the space between $z \approx -2$ and $+2 \text{ nm}$.

minor, and the electrolyte concentration turns out to be close to 0.5 M in all samples. For reasons that will be discussed below, the [bmim][Tf₂N] simulation has been repeated upon reducing the RTILs concentration by a factor of 2, considering a system of 80 ion pairs in 18651 water molecules.

Following the insertion of the RTILs ions, each system has been equilibrated during 30 ns, and then statistics has been collected over a time interval whose length is specified in Table 1. The relatively long equilibration time is needed to relax the configuration of the RTIL/water solution, and especially to reach a stationary distribution of ions across the system, a process that might require the diffusion of ions over lengths of the order of $L_z/2$. Convergence to equilibrium has been monitored by computing running averages of density profiles for the various species, of thermodynamic (volume) and mechanical (stress) properties.

The most intuitive and direct representation of the system behavior is given in Figure 7, showing simulation snapshots of the bilayer in contact with the [bmim][Cl], [bmim][PF₆], and [bmim][Tf₂N] water solutions. In the [bmim][Cl] case (Figure 7a), there is an apparent tendency of [bmim]⁺ to be incorporated into the bilayer, whereas the Cl⁻ anions remain in solution. Closer analysis of snapshots shows that [bmim]⁺ in the bilayer tends to be oriented in such a way to solvate their butyl tails into the nonpolar region of the bilayer, whereas the imidazolium ring remains closer to the polar POPC heads, where the screening of its positive charge is most effective.

The [bmim]⁺ concentration, penetration depth and orientation into the POPC bilayer is similar in the [bmim]-[PF₆] case. The anion distribution, instead, is different, with PF₆⁻ giving rise to a negatively charged thin film wetting the phospholipid surface. Cations incorporated into the bilayer and PF₆⁻ anions adsorbed at its surface are in equilibrium with a diffuse atmosphere of positive and negative ions in water solution. The anion film at the lipid/water interface is stabilized by the Coulomb attraction from the [bmim]⁺ ions in the bilayer, whose effect is amplified by the relatively low affinity of PF₆⁻ for water. The stability of the anions' layer, moreover, is enhanced by the attractive interaction of PF₆⁻ with the polar head of POPC, due to fairly strong Coulomb forces, and especially by dispersion interactions between this bulky and polarizable ion with the phospholipid head.

Finally, the snapshot for [bmim][Tf₂N] shows a completely different situation, since, in this case, the concentration of the added salt is above its solubility limit.²⁵ As a result, [bmim][Tf₂N], whose initial distribution in the water bath is fairly homogeneous, precipitates out of the solution, forming one or a few mesoscopic blobs, in equilibrium with a very dilute population of ions in solution. Remarkably, all blobs remain in close contact with the bilayer, probably because of its hydrophobic character. Limited penetration of ions in the bilayer is observed in this case, partly because of the reduced mobility of ions in the blob with respect to ions in solution, and, more importantly, because of the stabilization of cations and anions within the RTIL droplet due to Coulomb forces, decreasing the driving force toward penetration. Even more remarkably, at variance from the previous systems, in this third case we observe the penetration of a nearly equal number of cations and Tf₂N⁻ anions below the polar region of the bilayer (Figure 7c). The interactions stabilizing the association of anions with POPC are similar to those at play in the [bmim][PF₆] case, with, however, a different balance among them, since Coulomb interactions are weakened by the large

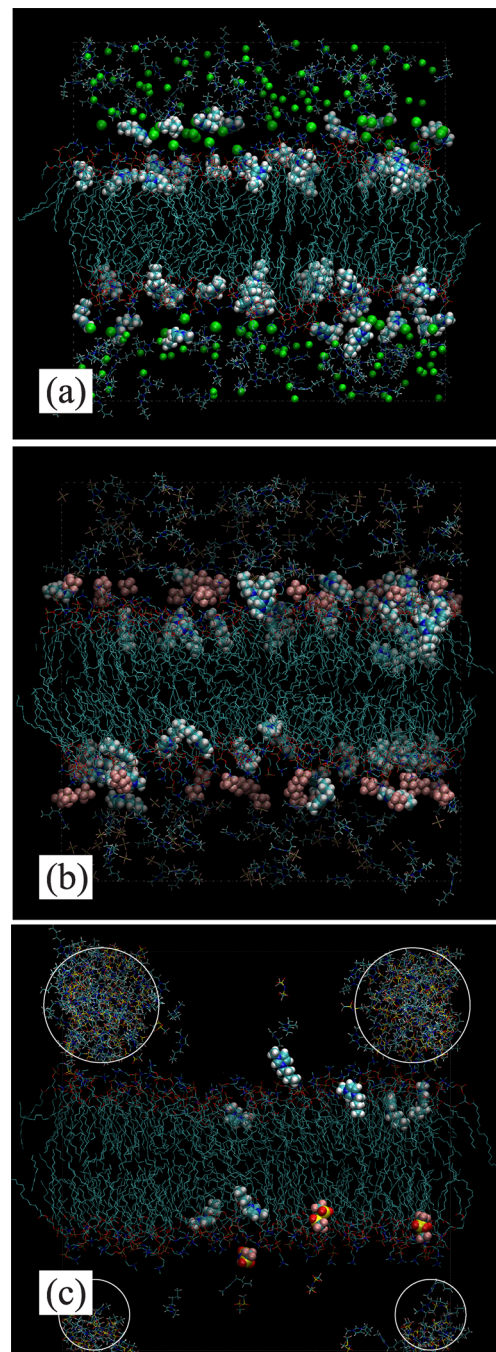


Figure 7. Simulation snapshots of a POPC bilayer in contact with a water solution of (a) [bmim][Cl], (b) [bmim][PF₆], and (c) [bmim][Tf₂N]. In all cases, a few ions close to or embedded into POPC have been highlighted, whereas the bulk of RTIL ions dissolved in water are drawn schematically. In the [bmim][Tf₂N] case, white circles identify accumulations of RTIL ions. The four blobs belong to a single droplet in contact with POPC and appear separated only because of periodic boundary conditions.

size of Tf₂N⁻, which at the same time enhances the dispersion interaction with the lipid tails. To increase the mobility and solvation (in water and/or in POPC) of ions in this last RTIL case, we repeated the [bmim][Tf₂N] simulation at half concentration (0.25 M). However, also in this case the segregation of the RTIL at the bilayer surface takes place within a few ns, and the simulation has been discontinued after a total of 40 ns (10 ns statistics).

Table 3. Average Values for the Area A_1 per Lipid Molecule (per Leaflet), Surface Compressibility Modulus κ_A , Interfacial Tension γ , Volume V_1 per Lipid Molecule Computed by the Test Particle Method (See Text), and Isothermal Compressibility χ_T Computed from the Fluctuations of V_1^a

solvent	A_1 (nm ²)	κ_A (mN/m)	γ (mN/m)	V_1 (nm ³)	χ_T (m ³ /J)
pure H ₂ O (w)	$0.59651 \pm 5 \times 10^{-5}$	0.590 ± 0.001	0.18 ± 0.05	$1.1876 \pm 3 \times 10^{-4}$	$(7.74 \pm 0.5) \times 10^{-10}$
[bmim][Cl]/w	$0.59771 \pm 6 \times 10^{-5}$	0.510 ± 0.002	0.15 ± 0.05	$1.2088 \pm 1 \times 10^{-3}$	$(1.11 \pm 0.05) \times 10^{-9}$
[bmim][PF ₆]/w	$0.60371 \pm 8 \times 10^{-5}$	0.325 ± 0.001	0.15 ± 0.05	$1.2075 \pm 1 \times 10^{-3}$	$(1.15 \pm 0.05) \times 10^{-9}$
[bmim][Tf ₂ N]/w (0.5 M)	$0.59245 \pm 6 \times 10^{-5}$	0.630 ± 0.001	0.15 ± 0.05	$1.1956 \pm 2 \times 10^{-4}$	$(7.47 \pm 0.05) \times 10^{-10}$
[bmim][Tf ₂ N]/w (0.25 M)	$0.6011 \pm 1 \times 10^{-4}$	1.030 ± 0.001	0.20 ± 0.05	$1.1962 \pm 3 \times 10^{-4}$	$(7.24 \pm 0.05) \times 10^{-10}$

^aThe nominal V_1 accounts also for the volume occupied by ions incorporated into the bilayer.

The qualitative picture shown in Figure 7 is confirmed and quantified by computing thermal averages for the quantities often used by the membrane-biophysics community to characterize the structure and dynamics of lipid bilayers. The main results have been collected in Table 3. The variations in the basic bilayer properties due to the addition of RTILs at 0.5 M concentration are relatively small, but in most cases well above the estimated error bar.⁵⁶ Moreover, the changes in going from the neat bilayer to the [bmim][Cl] case and then to [bmim][PF₆] are systematic, and easy to relate with the qualitative picture illustrated in Figure 7. The results for the [bmim][Tf₂N] solutions at 0.5 and 0.25 M are more erratic, partly because simulations have been discontinued soon after the beginning of the RTIL precipitation. Moreover and more importantly, the heterogeneous interface resulting from the segregation of [bmim][Tf₂N] at the lipid/electrolyte solution interface depends on the size and shape of the sample, and kinetic effects also play an important role.

The POPC bilayer in pure water, for instance, has an area of $0.59651 \pm 1 \times 10^{-5}$ nm² per lipid molecule in each leaflet, and an area compressibility modulus κ_A of 0.590 ± 0.001 mN/m. Adding [bmim][Cl] to the solution changes only slightly the area, increasing it by a fraction of a percent, while the change of κ_A (-15%) is more significant. The same trend is observed in the [bmim][PF₆] case, but both effects are quantitatively more important, with the κ_A variation reaching -45% . The effect of [bmim][Tf₂N] is the smallest among the systems that we considered. These trends are easily interpreted in terms of the morphology features shown in Figure 7. The stronger effect of [bmim][PF₆] as compared to that of [bmim][Cl], in particular, reflects the accumulation of both cations and anions within or at least close to POPC, whereas the limited effect of [bmim][Tf₂N] reflects its extensive segregation, lower ion mobility, and only partial wetting of the bilayer by the compact RTIL droplets, in which cations and anions are closely interacting with each other.

The volume V_t of the lipid bilayer estimated from the separation $\Delta_t = \{|Z_U - Z_L| - \sigma\}$ of the limiting surfaces increases nearly 2% in going from the pure water case to the [bmim][Cl] or [bmim][PF₆] solutions. In the [bmim][Cl] case, in particular, the volume change is $\delta V_t = 7.25$ nm³. To first approximation, we can assume that δV_t corresponds to the volume of the [bmim]⁺ cations incorporated into the bilayer. Moreover, since the [Cl]⁻ ions is certainly significantly smaller than [bmim]⁺, we approximate the volume of [bmim]⁺ with that of the entire [bmim][Cl] ion pair; that is, we set $v([bmim]^+) = v([bmim][Cl]) = 0.2683$ nm³, see section II. Then, we conclude that δV_t corresponds to the incorporation of ~ 25 [bmim]⁺ ions into POPC, a conclusion that is consistent with the number of ions in the bilayer seen in the simulation

snapshots. A similar estimate of 25 [bmim]⁺ ions in POPC is obtained in the [bmim][PF₆] case.

The enhanced disorder of the POPC distribution due to the incorporation of [bmim]⁺ is the most likely reason for the decreased surface compressibility modulus κ_A and parallel increase of isothermal volume compressibility χ_T and phospholipid diffusion constant (see Table 2, commented below) seen by simulation upon adding RTILs to the solution.

In addition to the area and volume expansion of the POPC bilayer due to the incorporation of [bmim]⁺ ions, a second, more subtle volume effect may provide further indications on the state of this complex system. We refer to the deviation of the total sample volume V_{tot} from the sum of the water, lipid and RTIL contributions. In this analysis, we take as a reference the volume per molecule v_w of pure water, of lipids (v_l) and of RTIL ion pairs (v_{ion}), the last two being computed independently in pure water solution (see section II). Then, the parameter $\delta^2 V = V_{tot} - n_w v_w - n_l v_l - n_{ions} v_{ions}$ measures the deviation from additivity in bringing the lipid bilayer in contact with the RTIL water solution. This deviation, in a way, represents a second order effect with respect to the δV_t variation of the lipid volume, which, to first order, is compensated by a $\sim -\delta V_t$ change in the volume occupied by the electrolyte solution, being due to the migration of the cations into the bilayer. The two contributions, however, do not cancel out exactly, and $\delta^2 V$ represents their difference. The simulation data show that $\delta^2 V$ is positive, i.e., the volume expands slightly, and the change is equivalent to the volume of 24 and 37 water molecules in [bmim][Cl] and [bmim][PF₆], respectively. Although relatively small, $\delta^2 V$ is significantly larger than the error bar. The systematic trend toward expansion suggests that the globally the system (slightly) loses cohesion upon putting the bilayer into the electrolyte solution, a change that has to be overcompensated by an increase in entropy. We do not know, at this stage, what kind of entropy is involved in the process, apart from an obvious contribution due to the mixing of [bmim]⁺ and lipids in the volume originally occupied by the bilayer. Further and longer computations are required to assess the role of the entropy of water, and of the entropy of the POPC tails. A check of the free energy balance by computing the enthalpy of the isolated component, unfortunately, is not trivial, because of the difficulty in defining and computing the enthalpy of the single components with respect to a consistent reference state. It might be worth mentioning that similar entropy effects have been discussed in ref 57 concerning the adsorption of Ca²⁺ ions at the lipid/water interface.

The diffusion constant of lipids, measured from the displacement of the P atoms, increases slightly in going from the pure water case to [bmim][Cl] and [bmim][PF₆]. The change is comparable to the error bar, and therefore no firm conclusion can be reached at this stage, but if confirmed, this

trend would be consistent with enhanced disorder and increase entropy in the lipid layer upon the addition of the RTIL ions.

The interfacial tension γ remains close to zero in all cases, again consistently with the picture of a liquid-like bilayer in contact with the solution.

Also the deuterium order parameter S_{CD} shows little changes upon the addition of RTILs to the solution, with differences among the different samples well within the estimated error bar. For completeness, we show the comparison between the pure water and RTIL solution results in a figure added to the Supporting Information.

The density profiles of water, POPC, cation and anion atoms, shown in Figure 8, once again reflect the morphology features

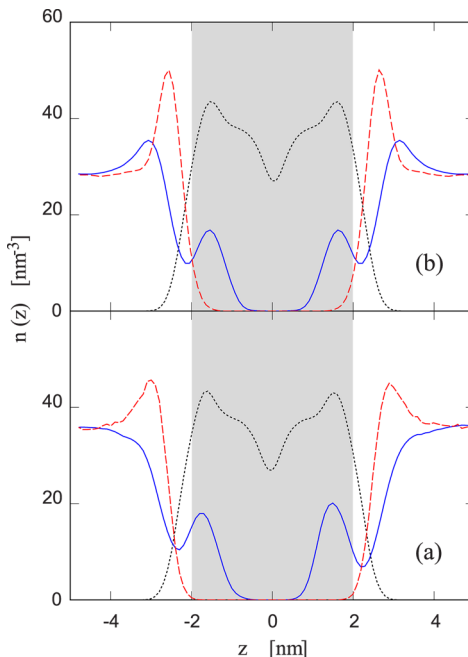


Figure 8. Density profile of POPC atoms (dotted line, black), cation (full line, blue) and anion (dash line, red) atoms obtained for the samples with (a) $[\text{bmim}][\text{Cl}]$ and (b) $[\text{bmim}][\text{PF}_6]$ in solution at 0.5 M concentration. For reasons of clarity, the density of $[\text{bmim}]^+$ atoms has been multiplied by 5; the density of $[\text{PF}_6]^-$ atoms has been multiplied by 18, and the $[\text{Cl}]^-$ density by a factor of 125.

shown in Figure 7. The density of $[\text{bmim}]^+$ atoms, for instance, is similar in the $[\text{bmim}][\text{Cl}]$ and in the $[\text{bmim}][\text{PF}_6]$ case, and clearly highlights the penetration of cations well within the geometric surfaces limiting the lipid bilayer. The density profile of anion atoms is different, since anions are nearly excluded from the bilayer, and the limited overlap with the POPC density profile might be due primarily to large amplitude, long wavelength oscillations of the lipid/electrolyte solution interface. Both in the $[\text{bmim}][\text{Cl}]$ and $[\text{bmim}][\text{PF}_6]$ case, the anion profile has a peak just outside the bilayer, probably due to the attraction of the positive charges intermixed with POPC. The anion peak is probably enhanced by excluded volume effects, analogous to those giving origin to the density pile-up outside a repulsive wall limiting the distribution of a hard sphere fluid. The anion peak is significantly taller and sharper in the $[\text{bmim}][\text{PF}_6]$ than in the $[\text{bmim}][\text{Cl}]$ case, reflecting the weaker affinity for water of $[\text{PF}_6]^-$ with respect to $[\text{Cl}]^-$. Apparently this results in the overscreening of the positive charge layer within POPC, giving raise, in turn, to the

accumulation of $[\text{bmim}]^+$ ions into a secondary peak on the solution side.

Comparison of the density (Figure 8) and of the charge density profiles (not shown), confirms that $[\text{bmim}]^+$ tends to be incorporated tail-first into the bilayer, i.e., solvating its butyl moiety into the hydrocarbon tails of POPC, keeping the ionic imidazolium ring close to the polar POPC head.

Remarkably, the separation of dissociated charges at the POPC/water interface does not cause a major change in the electrostatic potential across the bilayer (see Figure 9). The

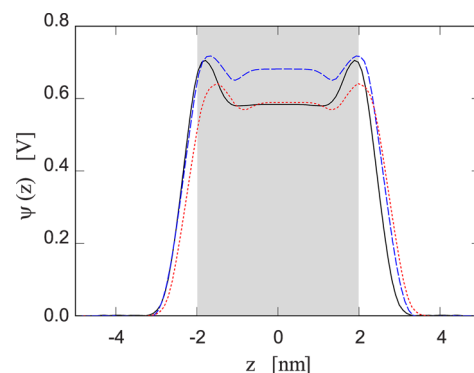


Figure 9. Comparison of the electrostatic potential $\psi(z)$ across the bilayer computed from the average charge density distribution for POPC in pure water (full line, black), POPC in contact with a $[\text{bmim}][\text{Cl}]$ 0.5 M solution (dash line, blue), and $[\text{bmim}][\text{PF}_6]$ 0.5 M solution (dotted line, red). The shaded area corresponds to the width of the POPC bilayer in pure water.

drop of the Coulomb potential between the inside and the outside of the bilayer, for instance, changes from $\Delta\psi = 0.58$ V in the pure water case, to $\Delta\psi = 0.68$ V for $[\text{bmim}][\text{Cl}]$ and to $\Delta\psi = 0.59$ V for $[\text{bmim}][\text{PF}_6]$. The relative stability of $\Delta\psi$ with changing strength of the electrolyte solution reflects the relatively low concentration of $[\text{bmim}][\text{Cl}]$ and $[\text{bmim}][\text{PF}_6]$, and, more importantly, the effective screening of electrostatic perturbation by water and by the polar head of POPC.

The vast amount of data accumulated during the simulation in the form of stored trajectories provides a wealth of detailed information on the system, guiding and confirming the analyses of the previous pages. We give here only two examples. Figure 10 shows the typical orientation of cations within the lipid

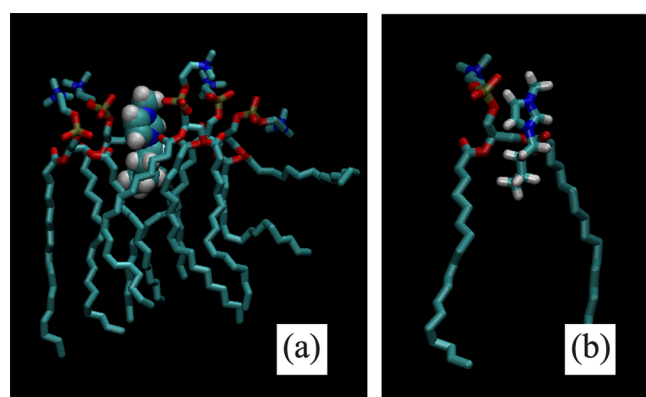


Figure 10. Simulation snapshot illustrating the relative position and orientation of $[\text{bmim}]^+$ embedded into the POPC bilayer. For the sake of clarity, the $[\text{bmim}]^+$ ion is drawn using two different styles in panels a and b.

layer, and illustrates the tendency of $[\text{bmim}]^+$ to enter the bilayer “tail-first”, optimizing the Coulomb and dispersion interactions with the POPC molecules. Figure 11, finally, shows

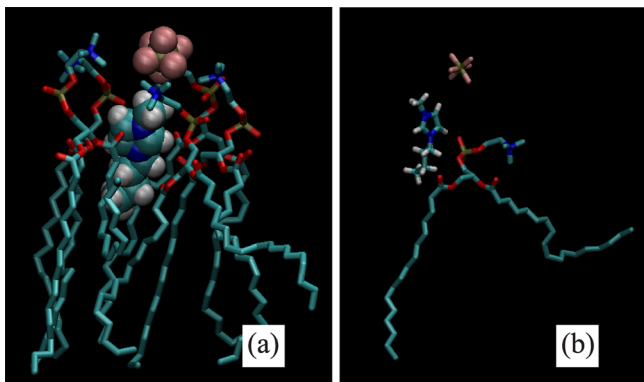


Figure 11. Simulation snapshots showing a typical configuration of $[\text{bmim}]^+$ and $[\text{PF}_6]^-$ ions at the POPC/water interface. For the sake of clarity, the $[\text{bmim}]^+[\text{PF}_6]^-$ ion pair is drawn using two different styles in panels a and b.

a typical configuration of $[\text{bmim}]^+[\text{PF}_6]^-$ ion pairs at the lipid/water interface, with $[\text{bmim}]^+$ surrounded by POPC, and $[\text{PF}_6]^-$ adsorbed but still outside the bilayer. As mentioned above, the relevance of the configurations shown in Figure 10 and in Figure 11 is confirmed by analysis and comparison of the number and charge density profiles.

IV. SUMMARY AND CONCLUSIONS

The interaction of a POPC bilayer with a water solution of $[\text{bmim}]^+[\text{Cl}]$, $[\text{bmim}]^+[\text{PF}_6]$, and $[\text{bmim}]^+[\text{Tf}_2\text{N}]$ at 0.5 M concentration has been investigated by molecular dynamics based on a classical empirical force field. An additional, short simulation has been carried out for POPC in a $[\text{bmim}]^+[\text{Tf}_2\text{N}]$ solution at reduced concentration (0.25 M). The computational framework is standard and corresponds to the state of the art in modeling fairly complex organic systems. However, to the best of our knowledge, our study represents the first application of these models to the investigation of phospholipid–RTIL solution interfaces and points to a new computational research direction that could provide important microscopic insight on the potential impact of RTILs on biomembranes.

The results of our simulations highlight important specific interactions of RTIL cations and anions with POPC, with trends and qualitative features reminiscent of the complex picture revealed by experiments.^{12,13,17,18} In $[\text{bmim}]^+[\text{Cl}]$ and $[\text{bmim}]^+[\text{PF}_6]$, the strongest effect on the POPC structure and stability is due to the incorporation into the lipid bilayer of the $[\text{bmim}]^+$ cation, whose position and orientation relative to the bilayer optimize both the solvation of the $[\text{bmim}]^+$ butyl tail within the hydrocarbon inner layer of POPC, as well as the screening of the imidazolium charge by the zwitterionic head of the phospholipid. Despite the strength of Coulomb forces between the RTIL ions, the interaction and fate of the anions largely depends on their interaction with water. Highly soluble species such as $[\text{Cl}]^-$ remain in solution, while the larger and less hydrophilic $[\text{PF}_6]^-$ anion gives rise to a thin film at the lipid/water interface. A different case is represented by the most hydrophobic of the three RTILs considered in our study, i.e., $[\text{bmim}]^+[\text{Tf}_2\text{N}]$, whose water solubility is limited to 0.02 M. Not surprisingly, both at 0.5 and 0.25 M concentration, the

$[\text{bmim}]^+[\text{Tf}_2\text{N}]$ solution, initially prepared in the homogeneous state, segregates one or a few RTIL droplets close to the lipid surface. Simulations at significantly lower $[\text{bmim}]^+[\text{Tf}_2\text{N}]$ concentration are not feasible in practice. In the segregated $[\text{bmim}]^+[\text{Tf}_2\text{N}]$ case, ions' penetration into the lipid bilayer is less extensive than in the $[\text{bmim}]^+[\text{Cl}]$ and $[\text{bmim}]^+[\text{PF}_6]$ samples, but still not negligible. Remarkably, $[\text{Tf}_2\text{N}]^-$ anions follow $[\text{bmim}]^+$ into the bilayer, and reside close to the intermediate region between the polar head and the hydrocarbon tails of POPC, driven by a combination of Coulomb, dispersion and hydrophobic interactions.

In the $[\text{bmim}]^+[\text{Cl}]$ and $[\text{bmim}]^+[\text{PF}_6]$ cases, the incorporation of $[\text{bmim}]^+$ into POPC is accompanied by a slight increase of the cross area of the bilayer and by a more significant (up to ~45%) decrease of its area compressibility modulus. Also the diffusion coefficient of phospholipids, measured in our simulations by the mean square displacement of P8 atoms in the POPC head, shows indications of a faster dynamics upon absorption of $[\text{bmim}]^+$, but in this case the relative change is only comparable to the error bar. A detailed analysis of the system volume in terms of the specific volumes of the water, lipid and RTIL components shows a small but significant positive deviation from additivity (or ideality upon mixing), a behavior usually associated to a slight increase of potential energy, which needs to be driven by a corresponding increase of the system entropy.

All these changes, i.e., the increase of the A_1 area and of χ_T , the decrease of κ_A , the quickening of diffusion and the increase in entropy, point to the destabilizing effect of $[\text{bmim}]^+[\text{Cl}]$ or $[\text{bmim}]^+[\text{PF}_6]$ on the POPC bilayer, which is consistent with the experimental findings.^{12,13,17,18}

The results for $[\text{bmim}]^+[\text{Tf}_2\text{N}]$ are more difficult to include into a systematic picture covering also $[\text{bmim}]^+[\text{Cl}]$ and $[\text{bmim}]^+[\text{PF}_6]$. However, the qualitative difference noted above, consisting in the incorporation of both cations and anions into the lipid bilayer, might be the reason behind the increased sensitivity of lipid membranes to $[\text{Tf}_2\text{N}]^-$ -based RTILs seen in experiments.

The results obtained in the present study confirm and reinforce those from a previous, very preliminary study,²³ carried out on an idealized lipid bilayer consisting of cholesterol molecules. The previous and present paper together explore only a tiny fraction of the systems and conditions of interest. Obvious directions for further investigations include the analysis of (i) other phospholipids, differing from POPC in their chemical identity and charge state, (ii) phospholipid mixtures, and phospholipid–cholesterol systems, and (iii) different RTILs, including both imidazolium systems with longer alkane chains, as well as RTILs not belonging to the imidazolium family. At a higher level of complexity, it would be important to include peptides and small proteins into the picture, considering first membrane proteins that need to work in an environment rich in lipids, which, in turn, could concentrate RTILs in their vicinity.

Our study raises a number of problems also concerning modeling and simulation. The force field used in our computations represents the state of the art in phospholipids and RTIL simulations but still provides only a very idealized view of the system and of its properties, and many improvements are required to reach quantitative accuracy in comparison with experiments. These could concern the inclusion of atomic polarizabilities, a better and more detailed parametrization of the lipid–RTIL interactions, and the

refinement of atomic charges by further ab initio studies. Longer simulations are needed as well, and coarse grained models are certainly required to reproduce the formation of holes and/or the extraction of lipids from the membrane by RTIL cations.

Already at the present stage, however, the results of our simulations provide a direct and intuitive view of the microscopic mechanisms underlying the effect of RTILs on phospholipid bilayers, at the same time highlighting the detail, reliability and realism reached by simulation approaches for systems as complex as phospholipid–RTIL solution interfaces.

■ ASSOCIATED CONTENT

§ Supporting Information

One figure showing the comparison of the NMR deuterium order parameter for the bilayer in pure water and in RTIL solutions; GROMACS topology files in plain text format for the POPC bilayer in the [bmim][PF₆] solution and in the [bmim][Tf₂N] solution; sample output configuration for the bilayer in pure water and in [bmim][Cl] solution. Running GROMACS for the systems considered in our simulations requires a few input files distributed by the [Web site](http://moose.bio.ucalgary.ca/), that are copied here in plain text format for the sake of completeness. This material is available free of charge via the Internet at <http://pubs.acs.org>.

■ AUTHOR INFORMATION

Corresponding Author

*Phone: +44(0)113-3439449. E-mail: r.j.bingham@leeds.ac.uk.

Notes

The authors declare no competing financial interest.

■ ACKNOWLEDGMENTS

Computations have been made possible by a Class 1b EPSRC-HPC grant. All simulations have been carried out using GROMACS 4.5.5/4.5.3, available on the Hector supercomputer. R.J.B. is supported by a Leverhulme Trust Research Grant (Grant no. RGSOMS480667).

■ REFERENCES

- (1) Welton, T. *Chem. Rev.* **1999**, *99*, 2071–2084.
- (2) Howlett, P. C.; MacFarlane, D. R.; Hollenkamp, A. F. *Electrochem. Solid-State Lett.* **2004**, *7*, A97–A101. Ishikawa, M.; Sugimoto, T.; Kikuta, M.; Ishiko, E.; Kono, M. *J. Power Sources* **2006**, *162*, 658–662.
- (3) Torimoto, T.; Tsuda, T.; Okazaki, K.; Kuwabata, S. *Adv. Mater.* **2010**, *22*, 1196–1221.
- (4) (a) Bonhôte, P.; Dias, A. P.; Papageorgiou, N.; Kalyanasundaram, K.; Grätzel, M. *Inorg. Chem.* **1996**, *35*, 1168–1178. (b) Papageorgiou, N.; Athanassov, Y.; Armand, M.; Bonhôte, P.; Pettersson, H.; Azam, A.; Grätzel, M. *J. Electrochem. Soc.* **1996**, *143*, 3099–3108. (c) Wang, P.; Zakeeruddin, S. M.; Exnar, I.; Grätzel, M. *Chem. Commun.* **2002**, 2972–2973.
- (5) Dupont, J.; de Souza, R. F.; Suarez, P. A. Z. *Chem. Rev.* **2002**, *102*, 3667–3691.
- (6) Ye, C.; Lui, W.; Chen, T.; Yu, L. *Chem. Commun.* **2001**, 2244. Nainaparampil, J. J.; Eapen, K. C.; Sanders, J. H.; Voevodin, A. A. J. *Microelectromech. Syst.* **2007**, *16*, 836–843.
- (7) Gurkan, B.; Goodrich, B. F.; Mindrup, E. M.; Ficke, L. E.; Massel, M.; Seo, S.; Senftle, T. P.; Wu, H.; Glaser, M. F.; Shah, J. K.; Maginn, E. J.; Brennecke, J. F.; Schneider, W. F. *J. Phys. Chem. Lett.* **2010**, *1*, 3494–3499.
- (8) Borra, E. F.; Seddiki, O.; Angel, R.; Eisenstein, D.; Hickson, P.; Seddon, K. R.; Worder, S. P. *Nature* **2007**, *447*, 979–981.
- (9) Wasserscheid, P.; Keim, W. *Angew. Chem., Int. Ed.* **2000**, *39*, 3772–3789. Fei, Z.; Geldbach, T. J.; Zhao, D.; Dyson, P. J. *J. Chem.—Eur. J.* **2006**, *12*, 2122–2130.
- (10) Holbrey, J.; Seddon, K. R. *Clean Products Processes* **1999**, *1*, 223–236.
- (11) Petkovic, M.; Seddon, K. R.; Rebelo, L. P. N.; Pereira, C. S. *Chem. Soc. Rev.* **2011**, *40*, 1383–1403.
- (12) Evans, K. O. *J. Phys. Chem. B* **2008**, *112*, 8558–8562.
- (13) DiCarlo, C. M.; Compton, D. L.; Evans, K. O.; Laszlo, J. A. *Bioelectrochemistry* **2006**, *68*, 134–143.
- (14) van Rantwijk, F.; Lau, R. M.; Sheldon, R. A. *Trends Biotechnol.* **2003**, *21*, 131–138. Kragl, U.; Eckstein, M.; Kaftzik, N. *Curr. Opin. Biotechnol.* **2002**, *13*, 565–571.
- (15) Pretti, C.; Chiappe, C.; Pieraccini, D.; Gregori, M.; Abramo, F.; Monnia, G.; Intorre, L. *Green Chem.* **2006**, *8*, 238–240.
- (16) Toxicology of RTILs has been experimentally investigated also in Bernot, R. J.; Brueseke, M. A.; Evans-White, M. A.; Lamberti, G. A. *Environ. Toxicol. Chem.* **2005**, *24*, 87–92. Viboud, S.; Papaaiconomou, N.; Cortesi, A.; Chatel, G.; Draye, M.; Fontvieille, D. *J. Hazardous Materials* **2012**, *215–216*, 40–48.
- (17) Evans, K. O. *Colloids Surf. A* **2006**, *274*, 11–17.
- (18) Evans, K. O. *Int. J. Mol. Sci.* **2008**, *9*, 498–511.
- (19) Berkowitz, M. L.; Vacha, R. *Acc. Chem. Res.* **2012**, *45*, 74–82.
- (20) Tatulian, S. A. In *Phospholipids Handbook*; Cevc, G., Ed.; Marcel Dekker: New York, 1993; pp 511–552.
- (21) Vernier, P. T.; Ziegler, M. J.; Dimova, R. *Langmuir* **2009**, *25*, 1020–1027.
- (22) Böckmann, R. A.; Hac, A.; Heimburg, T.; Grubmüller, H. *Biophys. J.* **2003**, *85*, 1647–1655.
- (23) Cromie, S. R. T.; Del Pópolo, M. G.; Ballone, P. *J. Phys. Chem. B* **2009**, *113*, 11642–11648.
- (24) See, for instance: Solomonov, I.; Weygand, M. J.; Kjaer, K.; Rapaport, H.; Leiserowitz, L. *Biophys. J.* **2005**, *88*, 1809–1817. Rapaport, H.; Kuzmenko, I.; Lafont, S.; Kjaer, K.; Howes, P. B.; Als-Nielsen, J. *Biophys. J.* **2001**, *81*, 2729–2736. Lafont, S.; Rapaport, H.; Sömjén, G. J.; Renault, A.; Howes, P. B.; Kjaer, K.; Als-Nielsen, J.; Leiserowitz, L.; Lahav, M. *J. Phys. Chem. B* **1998**, *102*, 761–765.
- (25) Toh, S. L. I.; McFarlane, J.; Tsouris, C.; DePaoli, D. W.; Luo, H.; Dai, S. *Solvent Extr. Ion Exch.* **2006**, *24*, 33–56. Crosthwaite, J. M.; Aki, S. N. V. K.; Maginn, E. J.; Brennecke, J. F. *J. Phys. Chem. B* **2004**, *108*, 5113–5119.
- (26) Tattrie, N. H.; Bennett, J. R.; Cyr, R. *Biochemistry* **1968**, *46*, 819–829.
- (27) Kučerka, N.; Tristram-Nagle, S.; Nagle, J. F. *J. Membr. Biol.* **2005**, *208*, 193–202.
- (28) Nagle, J. F.; Tristram-Nagle, S. *Biochim. Biophys. Acta* **2000**, *1469*, 159–195.
- (29) Leekumjorn, S.; Sum, A. K. *J. Phys. Chem. B* **2007**, *111*, 6026–6033. Ceccarelli, M.; Marchi, M. *Biochimie* **1998**, *80*, 415–419. Mauk, A. W.; Chaikof, E. L.; Ludovice, P. J. *Langmuir* **1998**, *14*, 5255–5266. Heller, H.; Schaefer, M.; Schulten, K. *J. Phys. Chem.* **1993**, *97*, 8343–8360.
- (30) Campbell, N. A.; Reece, J. B. *Biology*, 6th ed.; Benjamin Cummings: San Francisco, CA, 2001.
- (31) Hough, W. L.; Smiglik, M.; Rodríguez, H.; Swatloski, R. P.; Spear, S. K.; Daly, D. Y.; Pernak, J.; Grisel, J. E.; Carliss, R. D.; Soutullo, M. D.; Davis, J. H., Jr.; Rogers, R. D. *New J. Chem.* **2007**, *31*, 1429–1436.
- (32) Berendsen, H.; van der Spoel, D.; van Drunen, R. *Comput. Phys. Commun.* **1995**, *91*, 43–56. Lindahl, E.; Hess, B.; van der Spoel, D. *J. Mol. Mod.* **2001**, *7*, 306–317.
- (33) Berger, O.; Edholm, O.; Jähnig, F. *Biophys. J.* **1997**, *72*, 2002–2013.
- (34) Oostenbrink, C.; Villa, A.; Mark, A. E.; van Gunsteren, W. F. *J. Comput. Chem.* **2004**, *25*, 1656–1676.
- (35) Chiu, S.-W.; Clark, M.; Balaji, V.; Subramaniam, S.; Scott, H. L.; Jacobsson, E. *Biophys. J.* **1995**, *69*, 1230–1245.

- (36) Berendsen, H. J. C.; Postma, J. P. M.; van Gunsteren, W. F.; Hermans, J. In *Intermolecular forces*; Pullman, B., Eds.; D. Reidel Publishing Company: Dordrecht, The Netherland, 1981; pp 331–342.
- (37) Canongia Lopes, J. N.; Deschamps, J.; Padua, A. A. *H. J. Phys. Chem. B* **2004**, *108*, 2038–2047. Canongia Lopes, J. N.; Padua, A. A. *H. J. Phys. Chem. B* **2004**, *108*, 16893–16898. See also (Additions and corrections): Canongia Lopes, J. N.; Deschamps, J.; Padua, A. A. *H. J. Phys. Chem. B* **2004**, *108*, 11250–11250.
- (38) Bhargava, B. L.; Balasubramanian, S. *J. Chem. Phys.* **2007**, *127*, 114510. see also: Cremer, T.; Kolbeck, C.; Lovelock, K. R. J.; Paape, N.; Woelfel, R.; Schulz, P. S.; Wasserscheid, P.; Weber, H.; Thar, J.; Kirchner, B.; Maier, F.; Steinrueck, H. *Chem.—Eur. J.* **2010**, *16*, 9018–9030.
- (39) Pensado, A. S.; Malfreyt, P.; Padua, A. A. *H. J. Phys. Chem. B* **2009**, *113*, 14708–14718.
- (40) Bernardes, C. E. S.; Minas da Piedade, M. E.; Canongia Lopes, J. *N. J. Phys. Chem. B* **2011**, *115*, 2067–2074.
- (41) Pogor, D.; Mark, A. E. *J. Chem. Theory Comput.* **2010**, *6*, 325–336.
- (42) Tieleman, P. D.; MacCallum, J. L.; Ash, W. L.; Kandt, C.; Xu, Z.; Monticelli, L. *Journal of Physics: Condensed Matter* **2006**, *18*, S1221–S1234. See also the web site: <http://moose.bio.ucalgary.ca/>.
- (43) Darden, T.; York, D.; Pedersen, L. *J. Chem. Phys.* **1993**, *98*, 10089–10092. Essmann, U.; Perera, L.; Berkowitz, M. L.; Darden, T.; Lee, H.; Pedersen, L. G. *J. Chem. Phys.* **1995**, *103*, 8577–8592.
- (44) Hess, B.; Bekker, H.; Berendsen, H. J. C.; Fraaije, J. G. E. M. *J. Comput. Chem.* **1997**, *18*, 1463–1472.
- (45) Berendsen, H. J. C.; Postma, J. P. M.; van Gunsteren, W. F.; DiNola, A.; Haak, J. R. *J. Chem. Phys.* **1984**, *81*, 3684–3690.
- (46) Waheed, Q.; Edholm, O. *Biophys. J.* **2009**, *97*, 2754–2760.
- (47) Lindahl, E.; Edholm, O. *Biophys. J.* **2000**, *79*, 426–433.
- (48) See, for instance: Marrink, S. J.; Mark, A. E. *J. Phys. Chem. B* **2001**, *105*, 6122–6127. Farago, O. *J. Chem. Phys.* **2003**, *119*, 596–605. Cooke, I. R.; Kremer, K.; Deserno, M. *Phys. Rev. E* **2005**, *72*, 011506.
- (49) The difference is likely to be due to the different computational setup, and, in particular, to the different method to compute long-range Coulomb interactions (particle-mesh Ewald in our case, reaction field in ref 41), and perhaps a slightly different cutoff for Lennard-Jones potentials.
- (50) Pabst, G.; Rappolt, M.; Amenitsch, H.; Laggner, P. *Phys. Rev. E* **2000**, *62*, 4000–4009.
- (51) Smaby, J. M.; Momsen, M. M.; Brockman, H. L.; Brown, R. E. *Biophys. J.* **1997**, *73*, 1492–1505.
- (52) Seelig, A.; Seelig, J. *Biochemistry* **1977**, *16*, 45–50. Seelig, J.; Waespe-Šarčevč, N. *Biochemistry* **1978**, *17*, 3310–3315. Perly, B.; Smith, I. C. P.; Jarrell, H. C. *Biochemistry* **1985**, *24*, 1055–1063.
- (53) Lide, D. R., Ed.; CRC *Handbook of Chemistry and Physics*, 73 ed.; CRC Press Inc.: Boca Raton, FL, 1992.
- (54) Feller, S. E. *Curr. Opin. Colloid Interface Sci.* **2000**, *5*, 217–223. Kučerka, N.; Nagle, J. F.; Sachs, J. N.; Feller, S. E.; Pencer, J.; Jackson, A.; Katsaras, J. *Biophys. J.* **2008**, *95*, 2356–2367. Kučerka, N.; Tristram-Nagle, S.; Nagle, J. F. *Biophys. J.* **2006**, *90*, L83–L85.
- (55) Nagle, J. F.; Wiener, M. C. *Biochim. Biophys. Acta* **1988**, *942*, 1–10 see also ref 28..
- (56) The statistical error bar has been estimated by block averaging, upon dividing the run into 10 subintervals.
- (57) Binder, H.; Zschornig, O. *Chem. Phys. Lipids* **2002**, *115*, 39–61. Sinn, C. G.; Antonietti, M.; Dimova, R. *Colloids Surf. A: Physicochem. Eng. Aspects* **2006**, *282*, 410–419.